Waste Orange Peel–Derived Electrocatalysts for Efficient Air Cathodes in Zinc–Air Batteries

Alice Xinyi Li[1]

Received April 10, 2026
Accepted July 15, 2026
Electronic access August 15, 2026

Zinc-air batteries have attracted increasing attention as sustainable energy storage systems due to their high theoretical energy density and low cost. However, their practical application is limited by the reliance on expensive and scarce platinum-based catalysts. In this study, we aimed to develop an iron-doped biomass-derived electrocatalyst from waste orange peels through a high-temperature pyrolysis process. The structure and composition of the prepared catalyst were characterized using X-ray diffraction, scanning electron microscopy, nitrogen adsorption-desorption, and X-ray photoelectron spectroscopy. The oxygen reduction reaction performance of the catalyst was evaluated under alkaline conditions and further tested in zinc-air battery devices. The optimized catalyst showed good activity toward oxygen reduction, with a positive onset potential and a high current density. The assembled battery delivered an open-circuit voltage of 1.27 V and a maximum power density of 47 mW cm^{-2}. Moreover, three flow cells connected in series successfully powered a 3.0 V light-emitting diode wristband, demonstrating the practical feasibility of device integration. Although the performance remains lower than that of commercial Pt/C, further optimization is expected to enable this biomass-derived catalyst to serve as a sustainable and cost-effective alternative for zinc-air battery application.

Keywords: Waste orange peel, Biomass carbon, Electrocatalyst, Oxygen reduction reaction, Zinc-air batteries

Introduction

The world's rising demand for energy has caused severe resource depletion and environmental degradation, prompting the urgent need for the development of sustainable and efficient energy storage technologies[1,2]. However, conventional fossil fuel-based systems are being considered increasingly unsustainable, motivating the development of alternative energy storage solutions. Among various emerging technologies, metal-air batteries have gained attention as promising candidates for next-generation energy storage systems[3]. Zinc-air batteries (ZABs), in particular, stand out due to their large theoretical energy density, low production cost, and inherent safety[4,5]. The overall performance and efficiency of the ZABs largely depends on the oxygen reduction reaction (ORR) at the air cathode, which are often regarded as the primary limiting step due to its sluggish kinetics[6]. Therefore, the development of a highly efficient and durable electrocatalyst is essential for the practical application of ZABs in real life. Currently, extensive efforts have been devoted on to the synthesis of noble metal-based catalysts, particularly platinum-based materials, due to their supreme catalytic performance. However, despite this advantage, their high cost and low long-term stability under practical conditions significantly hinder large-scale applications[6,7].

Transition metal and nitrogen-doped carbon (M-N-C) materials have emerged as promising low-cost alternatives to noble metal-based ORR catalysts. Prepared via high temperature pyrolysis, these materials form numerous active sites from M-N_x coordination structures, which enhances their overall performance[8]. Most M-N-C catalysts are synthesized using commercial carbon materials such as carbon black and graphite as supports. However, metal aggregation remains a common problem faced during the synthesis process, as it reduces the accessibility of active sites and impairs catalytic activity and stability[9]. Recently, extensive efforts have been put on engineering the structure of the carbon support to obtain uniform M-N-C structures, including hollow carbon nanoparticles and carbon nanofibers, which have demonstrated excellent catalytic performance[10,11]. Nevertheless, the complex synthesis routes required by these catalysts still impede their scalability and cost-effectiveness, calling for the need of a simpler and more sustainable preparation route.

Biomass-derived carbon offers a sustainable and low-cost option for the development of catalysts due to their abundance and sustainability[12,13]. Compared to other biomass precursors, orange peels present as an attractive candidate as they are abundant in nature, inexpensive, and carbon rich. Un-

[1] *Overseas Chinese Academy of Concord Suzhou, China*

like coconut shells, banana peels, and lignin, which are common biomass materials used in electrocatalysis, orange peels possess a favorable biochemical composition and porous fibrous structure, enabling the formation of hierarchical porous and defect-rich carbon during pyrolysis[14]. Moreover, the use of orange peels reduces the reliance on conventional carbon sources and promotes waste recycling and sustainable resource utilization, making it a promising carbon precursor for the synthesis of efficient electrocatalysts for energy conversion applications.

Against this background, this study aims to propose a simple route for synthesizing efficient orange-peel derived electrocatalysts (OPC) for the air cathode in ZABs. It is hypothesized that waste orange peels, when carbonized and doped with a suitable amount of iron, can generate an efficient ORR catalyst for ZABs. By optimizing the Fe content, an active catalyst was synthesized. The resulting material was then systematically characterized in terms of structural characteristics, electrochemical performance, and practical applicability. Specifically, X-ray diffraction (XRD), scanning electron microscopy (SEM), nitrogen adsorption-desorption measurements, and X-ray photoelectron spectroscopy (XPS) will be used to analyze the catalyst's crystalline structure, surface morphology, pore characteristics, and elemental composition. The ORR performance and stability will be evaluated through standard electrochemical measurements to identify the optimal sample. In order to evaluate the practical performance of the OPC, the selected sample will be integrated into a ZAB device and the system's power density and stability are measured under repeated charge-discharge cycles. Ultimately, the system was used to power an LED band as a demonstration of its potential for real-world applications. The successful lighting of the band proves the practical potential of the synthesized catalyst.

Results

The OPC was synthesized through a two-step process involving pre-carbonization and iron doping. At first, the cleaned and dried orange peels were pre-carbonized in a tubular furnace at 400 °C for 2 h under an argon atmosphere to remove any moisture or volatile impurities. The pre-carbonized product was then ground into fine powder and dispersed in aqueous solutions containing different amounts of $Fe(ac)_2$ (1 wt%, 2.5 wt%, and 5 wt% relative to the biomass). After stirring for 24 hours, the suspensions were freeze-dried under vacuum to preserve the dispersion and structure of the Fe-containing precursor and minimize aggregation as the solvent was removed. The final powders were ultimately subjected to high temperature pyrolysis at 800 °C under a flowing 10% NH_3/Ar atmosphere, producing a series of Fe-doped OPC catalysts with varying iron contents.

The structure and morphology of the OPC samples were examined using XRD and SEM. The XRD patterns exhibit two broad peaks at 23.8° and 42.5°, which are the (002) and (101) planes of graphitic carbon (Figure 1a). The calculated interlayer spacing (d_{002}) of 0.376 nm indicates a relatively low degree of graphitization, which may be related to nitrogen incorporation and the resulting structural disorder within the carbon framework[15]. SEM images reveal a morphology dominated by carbon nanotube-like structures, accompanied by some particle aggregation in the OPC samples, with the relative proportion strongly dependent on Fe content doped. At a low Fe loading of 1.0 wt%, carbon nanotube-like structures are predominant, with only limited particle aggregation observed on the surface (Figure 1b). When the Fe loading is increased to 2.5 wt%, the particle aggregation becomes more evident while the nanotube-like morphology is still observable (Figure 1c). Further increasing the Fe content to 5.0 wt% results in extensive particle aggregation (Figure 1d).

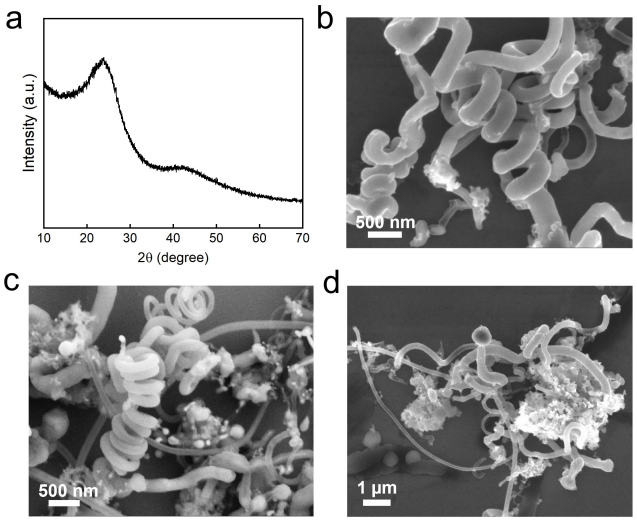

Figure. 1 Structural and morphological characterization of OPC samples. (a) XRD patterns of OPC catalyst. (b–d) SEM images of OPC samples with different Fe loadings: (b) 1.0 wt%, (c) 2.5 wt%, and (d) 5.0 wt%.

N_2 adsorption-desorption analysis was additionally performed to evaluate the specific surface area and pore structure of the OPC catalysts (Figure S1). The results show that the Fe-loaded OPC catalysts possess relatively high specific surface areas and a hierarchical porous structure. Notably, the 2.5 wt% Fe sample shows the highest specific surface area among all samples, which is expected to enhance mass transport and improve the accessibility of electrochemically active sites during the ORR process.

Elemental composition and chemical states of the OPC catalyst were further analyzed using XPS. The survey spectra

confirm the presence of C, N, and Fe in the sample. The C 1s spectrum can be deconvoluted into three peaks corresponding to graphitic sp^2 C–C (284.9 eV), C–O (285.7 eV), and O–C=O (287.5 eV), respectively (Figure 2a). The N 1s spectrum displays peaks at 398.1 eV, 399.2 eV, 401.0 eV and 404.6 eV, which are assigned to pyridinic-N, pyrrolic-N, graphitic-N, and oxidized-N, respectively [16] (Figure 2b). Pyridinic-N is generally considered to contribute to the formation of Fe-N_x centers and to modulate the local electronic structure of carbon matrix, which may facilitate oxygen adsorption and activation [17]. The peak at 398.8 eV peak, together with Fe 2p signals at 705.0 eV and 711.0 eV, is attributed to Fe-N coordination species (Figure 2c) [18,19].

The electrochemical ORR performance of the OPC catalysts was evaluated in an H-type cell using a standard three-electrode configuration (Figure S2). The catalyst was loaded onto carbon paper with a catalyst loading of 1 mg cm^{-2}, and 1 M KOH was used as the electrolyte under O_2-saturated or N_2-saturated conditions. In this setup, O_2 was supplied directly to the side of the working electrode, enabling simultaneous contact with the electrolyte and catalyst to form a three-phase interface. As expected, negligible current response was observed in N_2-saturated electrolyte, whereas a distinct cathodic current appeared under O_2-saturated conditions, indicating that the measured current originates from ORR (Figure 3a). For comparison, a Ketjenblack-loaded electrode was also tested and evaluated. The results showed that it exhibited a weak cathodic response, indicating a neglectable contribution from the carbon support under identical conditions (Figure S3). Among all the tested sample, the OPC (2.5 wt%) catalyst exhibited the best performance, giving an onset potential of 0.85 V versus reversible hydrogen electrode (RHE, hereafter). The current density significantly increased within the working potential range and reached 120 mA cm^{-2} at 0.2 V vs. RHE, indicating efficient ORR activity. The electrochemical performance of a commercial Pt/C catalyst was also tested under identical conditions as a benchmark reference (Figure S4). Although the OPC (2.5 wt%) showed lower ORR activity compared to the benchmark, its renewability and low cost still makes it a promising candidate for large-scale applications in the future.

The effect of Fe loading on ORR performance was then evaluated. Both the onset potential and current density were found to increase with Fe content, reaching a maximum at 2.5 wt% and decreasing at higher loadings (Figure 3b). Among the samples, the OPC catalyst with 2.5 wt% Fe exhibits the most positive onset potential of 0.85 V vs. RHE and the highest current density, which is therefore identified as the optimal composition within this study.

To further evaluate the ORR selectivity, rotating ring-disk electrode (RRDE) measurements were conducted to determine the electron transfer number (n) and H_2O_2 yield. The results suggest that the ORR predominantly proceeds via a four-electron pathway, with only a minor contribution from the two-electron pathway, indicating low H_2O_2 productions (Figure S5). The stability of the OPC catalyst was assessed by chronoamperometry at a constant potential of 0.67 V under O_2-saturated conditions. The current density remains nearly unchanged over 3600 s, implying good durability (Figure 3c).

Based on the promising ORR activity of the OPC catalysts, we assembled the synthesized catalyst into ZABs to evaluate their potential as air cathode materials. The devices employed OPC-loaded hydrophobic carbon paper as the air cathode, zinc foil as the anode, and 1 M KOH as the electrolyte, which was continuously circulated using peristaltic pumps (Figure 4a). The assembled ZAB delivers an open-circuit voltage of 1.27 V (Figure 4b). The polarization curve and corresponding power density curve show a maximum power density of approximately 47 mW cm^{-2} at a current density of 80 mA cm^{-2} and a cell voltage of 1.20 V (Figure 4c). At higher current densities, the voltage drops sharply, which is likely due to mass-transport limitations.

To further demonstrate practical applicability, three ZABs were connected in series. The combined open-circuit voltage increases to 3.72 V (Figure 4d), and a maximum power density of $\sim$115 mW cm^{-2} is achieved at 58 mA cm^{-2}, corresponding to an output voltage of 3.50 V (Figure 4e).

Finally, we demonstrated the practical applicability of the system by connecting three flow cells in series to power external electronic devices. The three-cell stack delivered a combined open-circuit voltage of 3.8 V, as measured by a multimeter, consistent with the expected additive scaling from single-cell operation (Figure 5a). As shown in Figure 5b-c, the stacked cells successfully powered a commercial LED wristband, providing stable illumination under both ambient light and dark conditions. The continuous lighting confirms that the stacked flow cells can provide sufficient output to drive low-voltage electronics. This demonstration shows that under real-world scenarios, multiple units can be integrated to potentially meet the high voltage and power requirements, while also validating the scalability of the flow cell architecture as well as the efficiency of the synthesized catalyst.

Discussion

In this study, Fe-doped OPC were successfully synthesized using waste orange peels with appropriate Fe-doping. Structural characterization showed the formation of a porous, CNT-predominant carbon framework, together with the presence of Fe-N_x active sites, which are likely to enhance the catalyst's performance. Among the three prepared samples, the OPC (2.5 wt%) exhibited the best ORR performance, delivering an onset potential of 0.85 V v.s. RHE and stable operations in the ZAB, with an open-circuit voltage of 1.27 V and a peak power

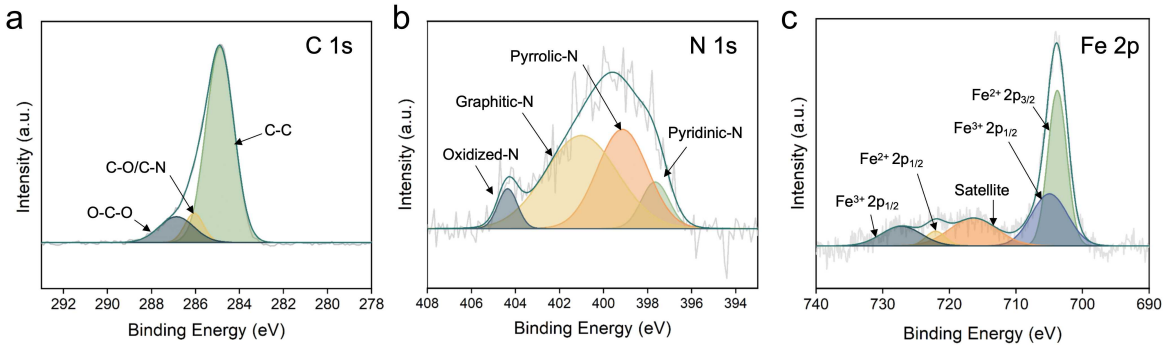

Figure. 2 XPS spectra of the OPC sample. (a) C 1s spectrum; (b) N 1s spectrum; (c) Fe 2p spectrum.

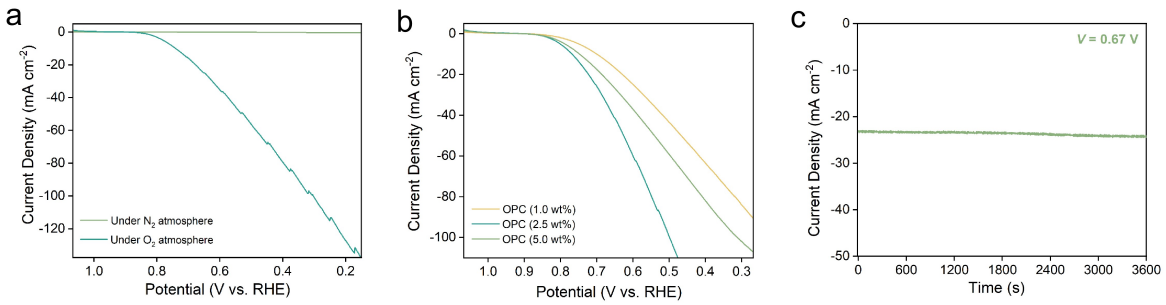

Figure. 3 Electrochemical ORR performance of OPC catalysts in H-cell. (a) Polarization curves of OPC (2.5 wt%) under different atmospheres. (b) Polarization curves of OPC catalysts with different Fe loadings. (c) Chronoamperometry response of OPC (2.5 wt%) at a constant potential of 0.67 V.

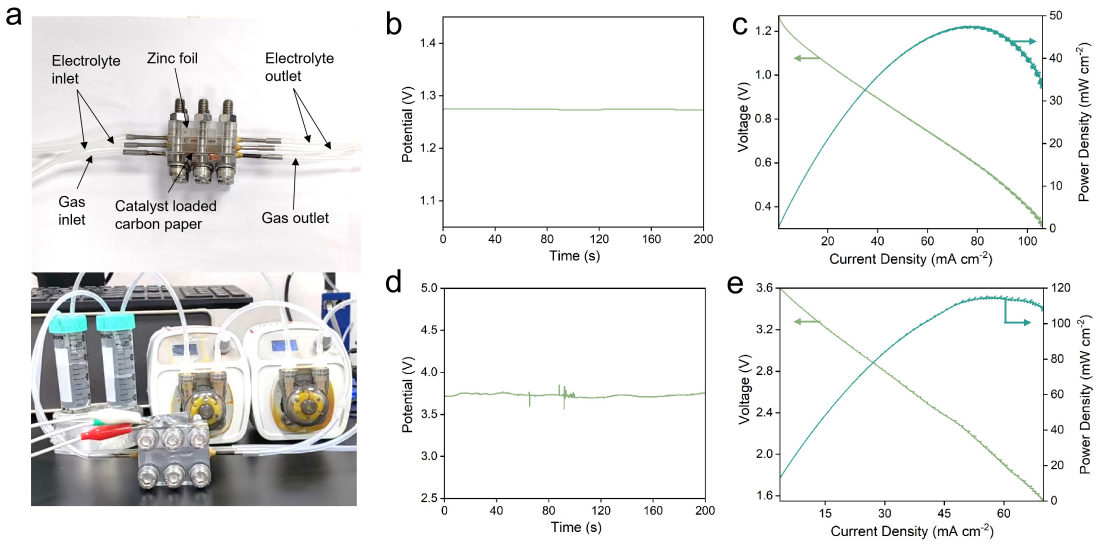

Figure. 4 Electrochemical performance of the ZAB device. (a) Photograph of the customized flow cell. (b) OCPT curve of a single ZAB. (b) Discharge polarization and power density curves of a single ZAB using OPC cathode. (c) OCPT of three ZABs connected in series. (d) Discharge polarization and power density three ZABs connected in series.

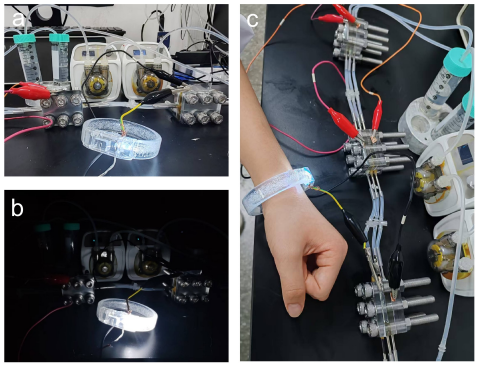

Figure. 5 Practical demonstration of theZAB-powered device. (a) Photograph of the LED wristband with lights on. (b) LED wristband in the off state for comparision. (c) LED wristband worn by the experimenter.

density of approximately 47 mW cm^{-2}. Ultimately, the successful operation of the three-cell stack to power a LED wrist band highlights the feasibility of the device for larger applications. Overall, the results from the experiment confirmed that orange peels can be converted to active electrocatalysts after high temperature carbonization and iron doping. Although its performance is still not comparable to the commercial Pt/C benchmarks, its advantages of low cost and renewability provides it the potential to serve as an alternative for ZABs in the future.

Structural analysis reveals the presence of both carbon nanotubes and aggregated particles, which can be attributed to the catalytic effect of Fe during high temperature carbonization[20]. During this process, carbon-containing gaseous species like CO and CH_4 was generated from the decomposition of orange peel biomass and could serve as additional carbon sources for CNT formation, as reported in previous studies[21,22]. These gas species will decompose on the surface of Fe nanoparticles within the OPC matrix, where carbon atoms adsorb and subsequently precipitate as graphitic layers, leading to the formation of tubular CNT structures via vapor-liquid-solid (VLS) or vapor-solid-solid (VSS) pathways[23]. The CNT formed is expected to improve the electrical conductivity of the material, which will potentially enhance its ORR performance. While Fe may play a role in CNT formation during pyrolysis, the enhanced electrocatalytic performance is still mainly associated with the formation of Fe-N_x active sites incorporated within the biomass-derived carbon framework. However, it's important to note that, the effect of Fe-doping on waste orange peels was the primarily area investigated in this study, with emphasis placed on optimizing the Fe content and assessing its effect on the catalyst's ORR performances. The dispersion of the Fe-N_x active sites, on the other hand, still remain unsolved. Future research could therefore focus on proposing synthetic routes that yields catalysts with a more uniform Fe-N_x distribution, which may further enhance its overall catalytic performance in advanced energy conversion systems.

Electrochemical testing confirmed the high ORR activity of the OPC catalysts, further supporting the hypothesis that orange peel-derived catalysts can serve as efficient air cathode materials for ZABs. Although the current performance of the catalyst may still not reach the most advanced reported catalysts, the use of kitchen waste as the precursor offers advantages in cost reduction and resource recycling. Notably, the ORR performance of the OPC showed a clear dependence on the amount of Fe doped. Moderate Fe incorporation showcased the best catalytic activity, which is likely due to the increased formation and more uniform dispersion of Fe-N_x active sites during pyrolysis. In contrast, excessive Fe content resulted in a decline in activity, possibly because of the presence of more particle aggregation that reduces the effective exposure and utilization of active sites.

At this stage, Fe incorporation was controlled only by adjusting the amount of Fe within the $Fe(ac)_2$ solution. Therefore, further optimization remains necessary when compared with the most effective and efficient catalysts reported in the literature[24,25]. In addition to Fe-N_x sites as the main active centers, the ORR activity may also be affected by other factors, including pore structure, electrical conductivity, nitrogen species distribution, and the presence of residual Fe-containing species. Together, these factors can affect mass transport and active site accessibility, thereby impacting the overall catalytic performance. Systematically optimizing the synthesis parameters, such as pyrolysis temperature and post-treatment processes (e.g., acid washing), would therefore be an aspect where further research is needed to achieve structural uniformity and catalytic efficiency for the OPC-based electrocatalysts.

Although ZABs have long been recognized as a promising energy storage technology, their application has been restricted by the absence of an efficient ORR catalyst at the cathode[26,27]. The assembly of OPC as the cathode material into a ZAB proves it practical potential. The effective voltage scaling demonstrates the feasibility of simple cell stacking to enhance output, while slight fluctuations in the open-circuit potential overtime indicate minor instabilities within the stack. Several factors may contribute to these fluctuations, including uneven liquid and gas distribution, interfacial contact resistance, and membrane hydration changes. These factors would collectively affect the transport of ions, causing signal variations and instabilities during the operation. The minor fluctuations may also be attributed to the non-ideal assembly conditions during the testing, as the current system only represents a proof-of-concept rather than a fully optimized design. Further optimization of the cell design will be needed in order to reduce the fluctuations.

Meanwhile, the current stability tests were limited to 3600 seconds, which is short relative to practical requirements. As the system operates for extended periods, it may experience performance decay caused by Fe leaching, carbon oxidation, or electrode flooding, which all reduces active site accessibility and hinder mass/electron transport within the electrode. Future studies could therefore extend the stability test to over hours or days in order to better understand the catalyst's performance under practical conditions. Addressing these limitations would give a comprehensive understanding of the OPC's practical potential to serve as ORR catalysts. All in all, through synthesis and systematic characterization of the OPC, this study underscores the feasibility of utilizing waste orange peels as the carbon precursor for efficient ORR catalysts, offering a promising candidate for green energy storage technologies in the future.

Methods

This study presents a simple route for synthesizing the orange-peel derived electrocatalyst that could be employed in ZABs. The OPCs are prepared with precisely controlled Fe-dopant (1.0 wt%, 2.5 wt%, and 5.0 wt%), which is the primary variable investigated, to gain a holistic understanding of how the amount of metal incorporation will influence the performance of the catalyst. XRD, SEM, BET, and XPS techniques are used to examine the structure and morphology of the yielded product, and its ORR performance was evaluated through standard electrochemical measurements. To further demonstrate the OPC's practical potential, it was integrated into a ZAB as the cathode material, and the system's power density and stability was measured. This experimental procedure allows for a comprehensive evaluation of the OPC's practical potential and enables the extrapolation of the relationship between metal incorporation and performance.

In this study, discarded orange peels were obtained from consumed oranges purchased from a local market. These peels were processed to produce different Fe-doped samples. The main difference among the samples is the Fe content. In addition, the other chemical reagents used in this study are listed as follows: Iron (II) acetate ($Fe(ac)_2$, 95%) was obtained from J&K Scientific Co., Ltd. Potassium hydroxide (KOH, 99%) was purchased from Macklin Biochemical Co., Ltd. (Shanghai, China). Commercial Pt/C (20 wt% platinum on Vulcan XC72) was purchased from Premetek Co. Ketjenblack carbon (KB, GR) was supplied by Huizhou Tenghui Technology Co., Ltd. Carbon fiber papers (P75T and 39BB) were provided by Suzhou Sinero Technology Co., Ltd., and the zinc foil was obtained from Suzhou Suke Jingyi Instrument Co., Ltd. Deionized water was prepared using a Milli-Q purification system and used throughout all experiments. All chemicals were purchased and used without further purification.

Preparation of OPC Catalyst

The leftover orange peels from eaten oranges were first air-dried at room temperature for several days until they became hard and brittle. The dried peels were then placed in clean plastic bags and soaked in deionized water, followed by ultrasonic treatment for 15 min to remove any impurities on the surface. After draining, the peels were immersed in anhydrous ethanol and ultrasonically treated for an additional 15 min to eliminate residual water and soluble organic compounds. The peels were subsequently rinsed with deionized water and subjected to a further 15 min of ultrasonic cleaning. Finally, thoroughly cleaned orange peels were transferred to a clean beaker and oven-dried at 80 °C for 24 h to remove surface moisture.

The dried orange peels were subjected to pre-carbonization in a tubular furnace under an Ar atmosphere. The temperature was ramped at a rate of 5 °C min^{-1} to 400 °C and maintained for 2 h. After pre-carbonization, the furnace was allowed to cool naturally to room temperature, and the obtained material was finely ground using a mortar and pestle. Subsequently, 0.5 g of orange peel powder was dispersed in 20 mL of ethanol solution containing $Fe(ac)_2$ at different loadings (1 wt%, 2.5 wt%, and 5.0 wt%, relative to the mass of orange peel powder) and stirred continuously for 24 h. The resulting mixtures were washed several times with deionized water and subsequently subjected to vacuum freeze-drying to obtain the OPC precursor powder. Finally, a total of 0.2 g of Fe-loaded OPC powder was carbonized in a tubular furnace by heating at 5 °C min^{-1} to 800 °C and holding for 1 h under a flowing 10% NH_3/Ar atmosphere, yielding Fe-doped OPC catalysts.

Structural Characterization

XRD analysis was conducted on a PANalytical X-ray diffractometer using monochromatic Cu Kα radiation (λ = 1.5406 Å). The diffraction patterns were recorded over a 2θ range of 5–80 ° with a step size of 0.026° and a scan rate of 0.067°/s. Data processing included background subtraction, peak fitting, and phase identification using the ICDD PDF-4 database and HighScore Plus (PANalytical).

SEM images were collected using a ZEISS G500 instrument. The accelerating voltage was set to 5.00–6.00 kV, with a working distance of 7.7–9.1 mm. Images were acquired over a magnification range of 9.21–39.21 K X. The samples were prepared by dispersing the material in ethanol, followed by drop-casting onto a silicon wafer and drying under ambient conditions.

BET analysis was performed on a Quantachrome Autosorb Station 1 instrument. Prior to measurements, the samples were degassed at 120 °C for 8 h under vacuum to remove adsorbed impurities. N_2 adsorption-desorption isotherms were recorded at 77 K using liquid nitrogen as the coolant. The spe-

cific surface area was calculated using the Brunauer-Emmett-Teller (BET) method based on adsorption data in the relative pressure (P/P_0) range of 0.05–0.30. The total pore volume was estimated from the nitrogen uptake at P/P_0 = 0.99. The pore size distribution was determined using the Barrett–Joyner–Halenda (BJH) method from the adsorption/desorption branches.

XPS analysis was performed on an SSI S-Probe XPS spectrometer using a Kratos Axis UltraDLD spectrometer (Kratos Analytical, Shimadzu group company) using a monochromatic Al Kα X-ray source (1486.6 eV). The analyzer pass energy was set to 40 eV, and all spectra were calibrated by referencing the C 1s peak at 284.8 eV. Peak deconvolution was carried out using Shirley background subtraction and Voigt (Gaussian-Lorentzian) peak fitting functions using CasaXPS software, with constraints applied to binding energy positions and FWHM. The samples were prepared by pressing the catalyst powder directly onto indium foil, forming a conductive sample holder for XPS measurements.

Electrochemical ORR Measurement

To prepare working electrode, a catalyst ink was prepared using 1 mg of OPC, 0.5 mg of KB, and 7.5 μL of 5 wt% Nafion solution dispersed in 250 μL of ethanol and sonicated for 30 min. The resulting ink was dropcast onto a 1 $\times$ 1 cm^2 carbon fiber paper (P75T) and dried under room temperature and pressure. Electrochemical ORR measurements were carried out in an H-cell using a standard three-electrode configuration controlled by a CHI 660E potentiostat. The OPC-loaded working electrode and a SCE reference electrode were positioned in the anodic compartment, while a graphite rod served as the counter electrode in the cathodic compartment. Each compartment contained 25 mL of electrolyte and was separated by an anion-exchange membrane (FAA-PK-130, from Suzhou Sinero Technology Co., Ltd, pre-activated in 1 M KOH). Prior to each test, the electrolyte was bubbled with O_2 for at least 20 min to achieve saturation, and a steady O_2 flow of 20 sccm was maintained over the solution during measurements to ensure continuous oxygen supply. Polarization curves were collected at a scan rate 10 mV s^{-1}, while chronoamperometry (i-t) was employed to assess its stability over time.

Electrochemical RRDE Measurement

For RRDE measurements, the catalyst ink was prepared in the same manner as for the H-cell measurements and drop-cast onto a glassy carbon disk electrode (5 mm diameter). The catalyst loading was controlled at 0.089 mg cm^{-2}, followed by drying under ambient conditions prior to electrochemical testing. The RRDE experiments were carried out in O_2-saturated 0.1 M KOH solution at a rotation speed of 1600 rpm using a standard three-electrode configuration. Linear sweep voltammetry (LSV) curves were collected at a scan rate of 10 mV s^{-1}, and the ring current was simultaneously recorded to calculate the electron transfer number and H_2O_2 yield.

Zinc-Air Battery Testing and Device Demonstration

Zinc-air battery tests were carried out using a custom-built three-compartment flow cell reactor with a reaction area of 1 cm^2. The reactor consisted of a gas chamber, a cathodic gas diffusion electrode (GDE, 39BB carbon paper loaded with the catalyst at $\sim$1.0 mg cm^{-2}, a typical loading used in standard ZAB testing), a catholyte chamber, a cation exchange membrane (FAA-PK-130), an anolyte chamber, and a zinc foil. Both the catholyte and anolyte chambers were supplied with 1 M KOH, circulated at a flow rate of 20 mL min^{-1} using peristaltic pumps. Meanwhile, O_2 was continuously delivered to the gas chamber at the rate of 40 sccm using a digital mass flow controller. Polarization data (V-i) were collected using linear sweep voltammetry at a scan rate of 50 mV s^{-1}, while the open-circuit potential was monitored as simultaneously collected. In addition to measurements on a single flow cell, electrochemical performance of three identical flow cells connected in series was also investigated. All measurements were conducted under the same conditions using the same instrumentation. For practical demonstration, three identical flow cells were connected in series and used to power a 3.0 V LED wristband. All devices were directly connected to the series configuration under the same experimental conditions as the electrochemical measurements, without additional circuitry.

References

1 B. K. Bose, Global energy scenario and impact of power electronics in 21st century. IEEE Transactions on Industrial Electronics. Vol. 60, pg. 2638-2651, 2012, https://doi.org/10.1109/TIE.2012.2203771.

2 R. S. W. J. C. J. K. S. P. B. G. W. C. J. D. J. R. O.-M. K. T. Levin, J. Bistline, Energy storage solutions to decarbonize electricity through enhanced capacity expansion modelling. Nature Energy. Vol. 8, pg. 1199-1208, 2023, https://doi.org/10.1038/s41560-023-01340-6.

3 J. C. F. Cheng, Metal–air batteries: From oxygen reduction electrochemistry to cathode catalysts. Chemical Society Reviews. Vol. 41, pg. 2172-2192, 2012, https://doi.org/10.1039/c1cs15228a.

4 X. X. Q. X. Q. Wang, S. Kaushik, Sustainable zinc–air battery chemistry: Advances, challenges and prospects. Chemical Society Reviews. Vol. 52, pg. 6139-6190, 2023, https://doi.org/10.1039/D2CS00684G.

5 Q. L. Y. W. Z. S. L. A. X. Zou, M. Tang, Carbon-based electrocatalysts for rechargeable Zn–air batteries: Design concepts, recent progress and

future perspectives. Energy & Environmental Science. Vol. 17, pg. 386-424, 2024, https://doi.org/10.1039/d3ee03059h.

6 B. W. B. H. K. Y. Y. C. L. Li, X. Tang, Advanced architectures of air electrodes in zinc–air batteries and hydrogen fuel cells. Advanced Materials. Vol. 36, pg. 2308326, 2024, https://doi.org/10.1002/adma.202308326.

7 H. F. Q. Liu, L. Wang, Research progress on the construction of synergistic electrocatalytic OER/ORR self-supporting cathodes for zinc–air batteries. Journal of Materials Chemistry A. Vol. 11, pg. 4400-4427, 2023, https://doi.org/10.1039/D2TA09626A.

8 F. K. T. W. R. S. S. S. J. S. Bates, M. R. Johnson, Heterogeneous M–N–C catalysts for aerobic oxidation reactions: Lessons from oxygen reduction electrocatalysts: Focus review. Chemical Reviews. Vol. 123, pg. 6233-6256, 2022, https://doi.org/10.1021/acs.chemrev.2c00424.

9 J. G. J. N. X. G. G. M. Q. Niu, B. Chen, Flexible, porous, and metal-heteroatom-doped carbon nanofibers as efficient ORR electrocatalysts for zn–air battery. Nano-Micro Letters. Vol. 11, pg. 8, 2019, https://doi.org/10.1007/s40820-019-0238-4.

10 Z.-Y. W. Y. X. Q. X. S.-H. Y. H.-L. J. Y.-Z. Chen, C. Wang, From bimetallic metal-organic framework to porous carbon: High surface area and multicomponent active dopants for excellent electrocatalysis. Advanced Materials. Vol. 27, pg. 5010-5016, 2015, https://doi.org/10.1002/adma.201502315.

11 T. A. R. Z. Q. X. Q. L. Zhu, W. Xia, Metal-organic framework-derived honeycomb-like open porous nanostructures as precious-metal-free catalysts for highly efficient oxygen electroreduction. Advanced Materials. pg. 6391-6398, 2016, https://doi.org/10.1002/adma.201600979.

12 P. Z. P. W. N. C. B. Q. L. Z. J. Y.-B. D. H. He, R. Zhang, Functional carbon from nature: Biomass-derived carbon materials and the recent progress of their applications. Advanced Science. Vol. 10, pg. 2205557, 2023, https://doi.org/10.1002/advs.202205557.

13 J. C. V. D. W. R. L. S. De, A. M. Balu, Biomass-derived porous carbon materials: Synthesis and catalytic applications. ChemCatChem. Vol. 7, pg. 1608-1629, 2015, https://doi.org/10.1002/cctc.201500081.

14 Y. M. W. E. A. A. J. R. W. S. S. Lam, R. K. Liew, Activated carbon for catalyst support from microwave pyrolysis of orange peel. Waste and Biomass Valorization. Vol. 8, pg. 2109-2119, 2017, https://doi.org/10.1007/s12649-016-9804-x.

15 M. Tagiri, A measurement of the graphitizing-degree by the X-ray powder diffractometer. The Journal of the Japanese Association of Mineralogists, Petrologists and Economic Geologists. Vol. 76, pg. 345-352, 1981, https://doi.org/10.2465/ganko1941.76.345.

16 S. M. S. C. W. Wang, Q. Jia, Recent insights into the oxygen-reduction electrocatalysis of Fe/N/C materials. ACS Catalysis. Vol. 9, pg. 10126-10141, 2019, https://doi.org/10.1021/acscatal.9b02583.

17 C. A. S. S. T. K. J. N. D. Guo, R. Shibuya, Active sites of nitrogen-doped carbon materials for oxygen reduction reaction clarified using model catalysts. Science. Vol. 351, pg. 361-365, 2016, https://doi.org/10.1126/science.aad0832.

18 Y.-W. L. H.-S. P. I.-A. C. K.-B. M. M.-C. K. S.-J. K. D.-H. K. J.-I. S. K.-W. P. D.-H. Kwak, S.-B. Han, Fe/N/S-doped mesoporous carbon nanostructures as electrocatalysts for oxygen reduction reaction in acid medium. Applied Catalysis B: Environmental. Vol. 203, pg. 889-898, 2017, https://doi.org/10.1016/j.apcatb.2016.10.084.

19 L. M. Z. J. J. G.-X. D. Y. H. Q. H.-J. L. Q. J. M. Xiao, J. Zhu, Microporous framework induced synthesis of single-atom dispersed Fe-N-C acidic ORR catalyst and its in situ reduced Fe-N4 active site identification revealed by X-ray absorption spectroscopy. ACS Catalysis. Vol. 8, pg. 2824-2832, 2018, https://doi.org/10.1021/acscatal.8b00138.

20 N. S. E. Kukovitsky, S. L'vov, VLS-growth of carbon nanotubes from the vapor. Chemical Physics Letters. Vol. 317, pg. 65-70, 2000, https://doi.org/10.1016/S0009-2614(99)01299-3.

21 D. S. S. J. P. Tessonnier, Recent progress on the growth mechanism of carbon nanotubes: A review. ChemSusChem. Vol. 4, pg. 824-847, 2011, https://doi.org/10.1002/cssc.201100175.

22 M. S. E. T. K. O. S. Takenaka, M. Ishida, Formation of carbon nanofibers and carbon nanotubes through methane decomposition over supported cobalt catalysts. The Journal of Physical Chemistry B. Vol. 108, pg. 11464-11472, 2004, https://doi.org/10.1021/jp048827t.

23 C. J. J. Sengupta, The effect of Fe and Ni catalysts on the growth of multiwalled carbon nanotubes using chemical vapor deposition. Journal of Nanoparticle Research. Vol. 12, pg. 457-465, 2010, https://doi.org/10.1007/s11051-009-9667-1.

24 Y. L. T. L. G. N.-H. L. Z. L. M. L. K. Liu, J. Fu, Insights into the activity of single-atom Fe–N–C catalysts for oxygen reduction reaction. Nature Communications. Vol. 13, pg. 2075, 2022, https://www.nature.com/articles/s41467-022-29797-1.

25 J. Z. Z. L. H. X.-B. L. Z. Z. J. M.-S. M. Q. Ma, H. Jin, Stabilizing Fe–N–C catalysts as model for oxygen reduction reaction. Advanced Science. Vol. 8, pg. 2102209, 2021, https://doi.org/10.1002/advs.202102209.

26 H. D. Y. Li, Recent advances in zinc–air batteries. Chemical Society Reviews. Vol. 43, pg. 5257-5275, 2014, https://doi.org/10.1039/C4CS00015C.

27 F. Z. K. N. N. H.-X. W. W. H. X. S.-J. Z. Y. L. M. Zeng, Y. Liu, Metallic cobalt nanoparticles encapsulated in nitrogen-enriched graphene shells: Its bifunctional electrocatalysis and application in zinc–air batteries. Advanced Functional Materials. Vol. 26, pg. 4397-4404, 2016, https://doi.org/10.1002/adfm.201600636.

Supplementary information

The online version contains supplementary material available at https://nhsjs.com/?p=45064